


EXPERIMENTAL RELATIONSHIPS OF CLAY GOUGE
TO FAULTED ROCK PROPERTIES

by

William T. Hudgins III
Department of Geophysics

Submitted in Partial Fulfillment of the Requirements of the
University Undergraduate Fellows Program
1977-1978

Approved by:


John M. Logan, Ph.D., Faculty Advisor

Abstract

Weak clay minerals have been suggested as important members of fault gouge to explain aseismic creep. The Bombolakis silt-clay model seeks to account for aseismic creep and recurrent stress drops along natural faults by the electrical orientation of clay sheets and thixotropic hardening. Experimental evidence here using bentonite clay supports the Bombolakis model, and further, the relationships of water content, clay content, and the amount of previous shear are indicated as the primary factors influencing the stable sliding behavior of silt-clay and pure clay gouges.

The silt fraction dominates the pre-sliding frictional characteristics while the clay reduces the peak shear stress and dominates the stability of the sliding mode. Clay content appears to enhance the homogeneity of deformation within the gouge whether dry or saturated. Water content in the silt-clay system imposes a weakened, initial, non-linear yield on the saturated specimen but decreases in effect with further shear displacement. A significant work-hardening characterizes the sliding behavior of silt-clay gouges containing at least 50% clay. The presence of this behavior depends upon the content of 50% or more clay by volume to insure that deformation takes place within the gouge and not just at the gouge-rock interface.

Acknowledgements

I would like to thank Dr. John M. Logan for his participation in the University Undergraduate Fellows Program as my advisor and Group IV co-chairman. Much of the basic knowledge I needed to begin this project were provided by him as well as help and encouragement along the way. Also due thanks are Larry Teufel and Nigel Higgs who devoted valuable time to discussion and supervision. Special thanks go to Chris Brooks who typed most of the final draft and who drew beautiful diagrams in a short time.

The rock deformation apparatus was made available by the Center for Tectonophysics, Texas A&M University.

TABLE OF CONTENTS

	PAGE
INTRODUCTION	1
PREVIOUS STUDIES	4
EXPERIMENTAL PROCEDURE	10
EXPERIMENTAL RESULTS	13
DISCUSSION OF RESULTS	40
SUMMARY - CONCLUSION	44
APPENDIX	46

LIST OF FIGURES

FIGURE		PAGE
1	A schematic diagram after Bombolakis (1978) showing the plasticity index and clay fabrics	8
2	A schematic diagram after Bombolakis (1978) showing an example of the mobilization of effective friction during progressive shear	9
3	A schematic diagram after Bombolakis (1978) showing the recurrence deformation model for saturated pure clays	9
4	A schematic diagram showing the axial loading device (LSR)	12
5a	Stress and frictional coefficient vs. axial shortening; stress accumulation rate; 100% bentonite, dry	17
5b	Stress and frictional coefficient vs. axial shortening; stress accumulation rate; 100% bentonite, saturated	19
6a	Stress and frictional coefficient vs. axial shortening; stress accumulation rate; 50% bentonite, 50% calcite, dry	21
6b	Stress and frictional coefficient vs. axial shortening; stress accumulation rate; 50% bentonite, 50% calcite, saturated	23
7a	Stress vs. axial shortening; stress accumulation rate; 10% bentonite, 90% calcite, dry	25
7b	Stress and frictional coefficient vs. axial shortening; stress accumulation rate; 10% bentonite, 90% calcite, saturated	27
8	Stress and frictional coefficient vs. axial shortening; stress accumulation rate; 100% calcite, dry	29

LIST OF FIGURES (continued)

FIGURE		PAGE
9	Stress and frictional coefficient vs. axial shortening; comparison of 100% bentonite dry and saturated	31
10	Stress and frictional coefficient vs. axial shortening; comparison of 50% bentonite, 50% calcite dry and saturated	33
11	Stress vs. axial shortening; comparison of 10% bentonite, 90% calcite dry and saturated	35
12	Stress and frictional coefficient vs. axial shortening; varied compositions, dry	37
13	Stress and frictional coefficient vs. axial shortening; varied compositions, saturated	39

INTRODUCTION

Earthquakes are releases of seismic energy caused by the slip-page of crustal blocks along a zone of high stress concentration. The properties of the rock along this faulted zone are of primary interest to those who study earthquake prediction and control. Kisslinger (1974) has described the parameters involved in these properties as functions of the relative motions of the Earth's crust and mantle, the rate of strain accumulation in rocks, and their strengths. However, the knowledge of these in situ conditions is limited to indirect geological observation and gross geophysical measurements. Every conceivable avenue into the development of a coherent prediction program is being investigated, including the abnormal behavior of some animals prior to large seismic events. The trust in physical studies, however, is dependent largely upon the accuracy with which experimental and theoretical data can duplicate the measured behavior of earthquakes. Numerous theoretical models exist, based upon current physical and chemical laboratory tests which may vary any number of parameters deemed significant by field observation of known active faults.

Inherent in any such model must be the provision for a sliding surface behavior called "stick-slip". This describes what most earth scientists think is the process by which strained rocks along a pre-existing fault are displaced in a jerky motion, releasing stored stress and resulting in seismic events, or earthquakes. In fact, most

The citations on the following pages follow the style of The Geological Society of America Bulletin.

earthquakes originate along such pre-existing faults, and in the case of the San Andreas fault system, occur within 15 km. of the surface. Knowledge of this type helps to delimit the range of physical and chemical parameters that must be varied to test their relation to the creation of stick-slip displacement in the laboratory.

Once displacement has occurred along a fault, frictional debris, called gouge, is present and may influence the ability of this zone to accumulate further stress. The displacement along some active earthquake prone systems is very large. For instance, the total relative displacement along the San Andreas fault can be measured in terms of over 100 miles. The frictional characteristics of gouge then clearly must be a factor in understanding the characteristic stress accumulation in pre-existing faults prior to earthquakes.

One conclusion as to the interaction of mineral grains in gouge has associated stable sliding with low percentage mixtures of very weak minerals and those of much greater instability. Wu (1975) reported compositions in surface exposures of gouge collected from the San Andreas fault to be high in percentages of clay minerals ($\sim 20-40\%$). The existence of such large percentages of clay, even though in exposures subjected to weathering, prompts a special interest in the role of clay in the deformation mechanisms of pure and mixed gouges. Clay minerals, such as vermiculite and montmorillonite contain water layers between sheet structures of extremely fine grain size. Bombolakis has suggested a fault creep and stress drop model for saturated silt-clay gouges. It requires the existence of at least 60% silt (that is, clastic particles) in a supportive, homogeneous framework. This

framework allows the silica sheets in clay to undergo thixotropic hardening, a rotation to an interlocking partial electrical equilibrium, during periods of shear stress relaxation.

The purpose of this report is to investigate the effect of sodium montmorillonite (bentonite) on the sliding behavior of gouges containing various percentages of an unstable mineral (calcite). Several experiments were performed under saturated conditions in order to observe the effect of this clay's capacity for the absorption of water on the frictional characteristics of mixed gouge. The pure clay and silt-clay gouge models suggested by Bombolakis (1978) are used as a tentative background for the partial interpretation of stress/strain curves. The validity of these interpretations remains to be seen, pending the outcome of experimental Berea/Tennessee Sandstone precuts without gouge and microscopic evaluation of post-deformational structure in the silt-clay gouge specimen.

PREVIOUS STUDIES

Experimental

Results (Shimamoto, 1976) associate stable sliding in gouge with low percentage mixtures of weak clay minerals and those of much greater instability. It has also been indicated that gouge minerals of intermediate hardness, such as apatite, dolomite, and calcite, under dry conditions, are associated with the most unstable behavior (i.e. stick-slip). Quartz, orthoclase, and pyrite, harder minerals, have shown stable sliding up to 200 MPa confining pressure. Minerals with hardness approximately below 3 on Moh's hardness scale generally exhibit only stable sliding in triaxial tests. Hardness, however, has not proven to be a unique or necessary determinant in the sliding behavior of monomineralic gouges. There may also be layering or mixing of the different mineral grains and sizes coincident with displacement in polymineralic gouges. Conditions at the gouge-rock interface may be saturated or dry, or may alternate with the influx of pore fluids suggested to occur prior to some earthquakes due to dilatancy.

Under dry laboratory conditions, the bentonites dominate the behavior of gouge composed of equal portions of kaolinite, illite, chlorite, calcium bentonite, and sodium bentonite. It should be noted that gouges composed of illite and kaolinite behave similarly to those composed of quartz or crushed granite, and exhibit stick-slip at high confining pressures. However, those clay minerals having sheet structures, such as montmorillonite or vermiculite, exhibit stable sliding and very low friction as high as 600 MPa confining pressure.

Shimamoto hypothesized that bentonites, when present with minerals of higher shear strength, tend to become mixed with these stronger materials. Different percentages of dry, homogeneously mixed, clay with unstable minerals have been investigated (ibid.) in terms of their ability to inhibit stick-slip. In the case of sodium montmorillonite (Wyoming Bentonite), this stabilizing effect on anhydrite takes place for as little as 15% bentonite by volume. Further, the stabilizing effect of a clay on an unstable mineral seems related to its frictional strength. However, layering of the clay within the fault zone dramatically increases the stabilizing effect due to the internal structure of the layering.

Theoretical

The depth of our understanding of the deformation mechanisms present in clay dominated gouges may be represented by the accuracy of a theoretical model. Bombolokis (1978) has presented a fault creep and stress drop model for saturated silt-clay gouge. This model attempts to account for the dominant mode of displacement along the San Andreas fault (aseismic creep) in a way which also allows recurrent seismic events. It is assumed that due to the huge amount of displacement along the San Andreas Fault, brittle gouge minerals have, in many cases, reached a minimum particle size and are no longer susceptible to producing large stress drops from high-pressure granulation. It is intrinsic then to the development of the model, that the behavior of the colloidal fraction of sheet structure minerals in a saturated gouge may lead to instabilities which eventually result in stress drops.

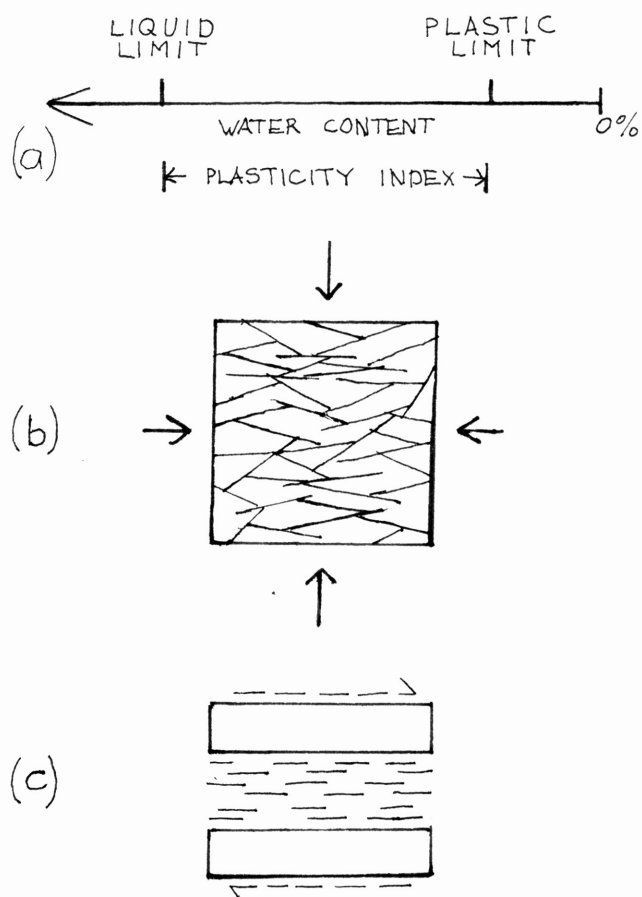
The gouge would consist of three phases: the brittle silt-sized particles, the free pore water, and the clay and colloidal size particles of sheet structure minerals with their absorbed water. Electrical forces on the tiny sheets result in ion adsorption and the development of a diffuse double layer of absorbed water. Mechanical properties of the clay change greatly as more water is absorbed. (Figure 1a) shows the Atterburg plastic and liquid limits as the content of water in a pure clay is increased (ibid.). The plastic limit defines where the clay deforms at its residual strength without crumbling, and the liquid limit defines that minimum point where the material displays the short term properties of a liquid. This range is the plasticity index, i.e. the range over which the residual shear is a property of the water content. (Figure 1b) represents the 'salt' type flocculated structure which seems to be mechanically stable to very large (300 MPa) effective stresses. Once shear strains have become sufficiently large for deformation to reach the residual strength, the platelets transform to the dispersed structure of (Figure 1c).

The frictional contacts are initially face-to-face with electroviscosity controlling the resistance to shear. Displacement under this mode is clearly time dependent. Viscous contacts have a limited lifetime, whereupon effective friction between the platelets themselves takes place. (Figure 2) shows (ibid.) how the mobilization of the effective friction takes place during shear. Only after this time-dependent mobilization can total collapse of the flocculated structure occur. Failure is then damped by the remaining effective cohesion.

Although no cyclic experiments were done in this research, the

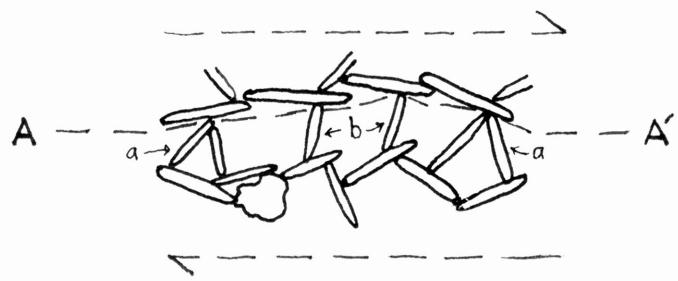
following discussion provides an extremely visual appreciation of the gouge model. A recurrence deformation sequence (ibid.) is described by (Figure 3). Strain hardening leads to a peak, subsequent stress drop, and dispersed structure, as shown in episode 1. A period of shear stress relaxation then allows thixotropic hardening to occur. This describes an electrical reorientation of the clay platelets into a 'salt' type flocculated structure. Deformation once again occurs, and the platelets are rotated to a dilatant 'cardhouse' structure at the peak stress in episode 2. The 'cardhouse' fails, and a dispersed orientation again results.

For thixotropic hardening to occur, a supportive silt framework must maintain the effective stress below 10 MPa in the colloidal phase. This requires 60% silt content for reasons outlined in the Bombolakis article (ibid.). The mechanism of failure in such a layer is not yet clear; however, it may involve the transformation of the gouge to a semiliquid condition due to locally high pore pressures.



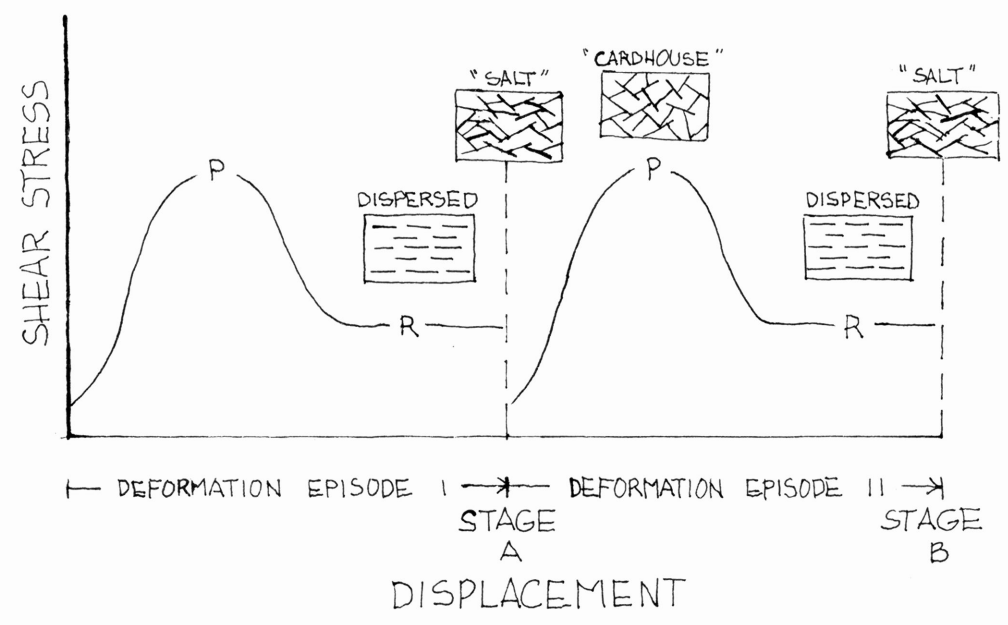
Plasticity index and clay fabrics. (a) Relation between plasticity index and the Atterburg liquid and plastic limits. (b) A 'salt' type flocculated structure in pure saturated clay. Arrows represent state of stress during consolidation. (c) Dispersed structure developed by extensive shear displacement (dashed arrows). Each colloidal clay platelet is surrounded by adsorbed water.

FIGURE 1



Example of the mobilization of effective friction during progressive shear (after Bjerrum, 1974). Clay platelets a are locked in position. Platelets b must rotate into a locked position during progressive shear before their full effective friction is mobilized.

FIGURE 2



Recurrence deformation model for saturated pure clays. Thixotropic hardening occurs during stages A and B, which represent quiescent periods separating deformation episodes.

FIGURE 3

EXPERIMENTAL PROCEDURE

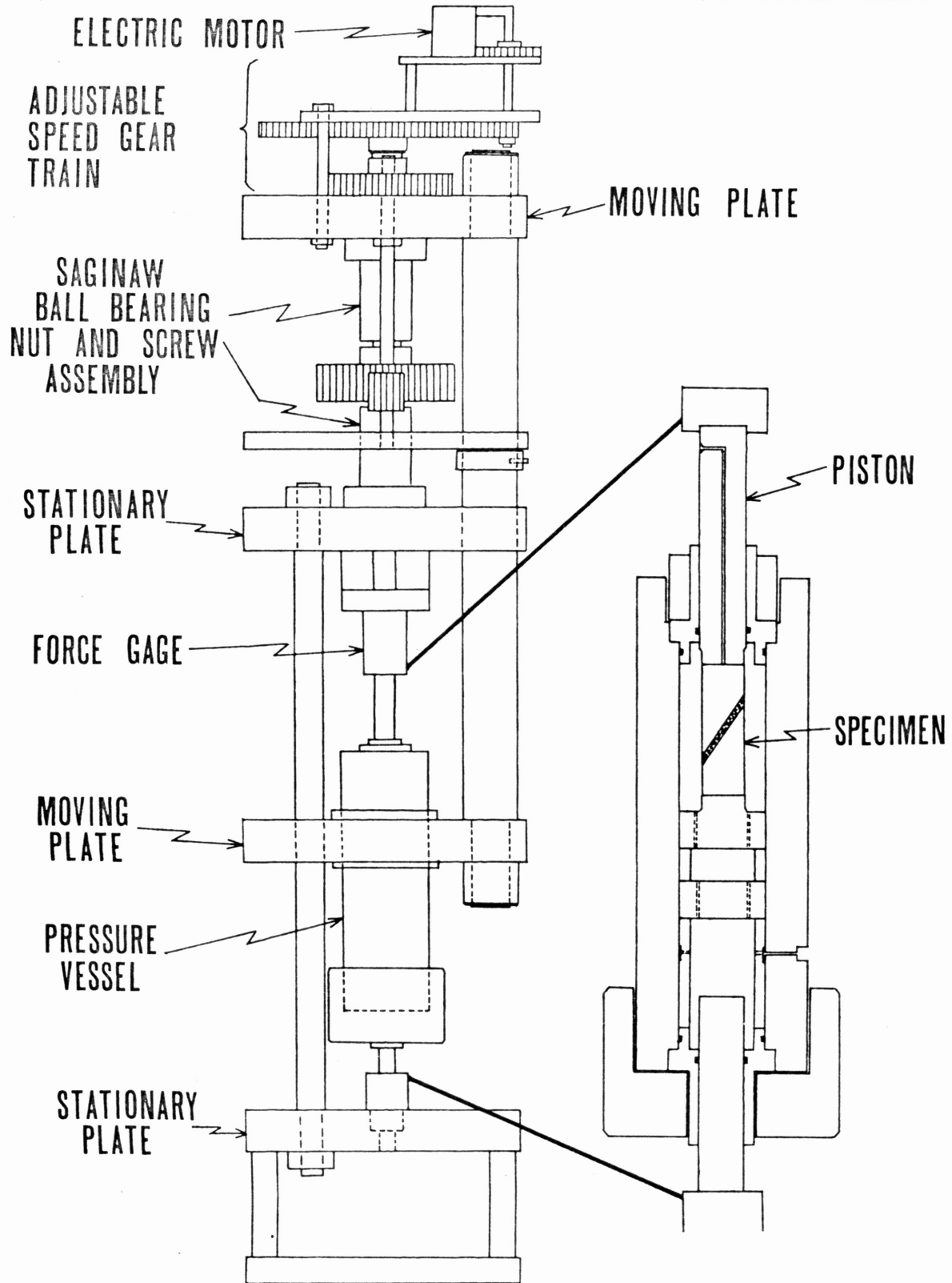
Right circular cylindrical specimens of Berea and Tennessee Sandstone were sawcut at 35° to provide halves for seven dilithologic experiments. Berea Sandstone was used as the upper member and Tennessee as the lower in all experiments in which the displacement rates $((2-5) \times 10^{-4}$ cm/sec) and effective confining pressures (100 MPa) were held constant at room temperature. Pore pressures in saturated experiments were constant at 10 MPa.

Berea Sandstone was used, despite its weakness compared to Tennessee Sandstone, to achieve good communication of pore fluids to the interface. Five polyolefin jackets were used around each specimen, and molycote lubricant was used on all end surfaces except where it would interfere with the communication of pore fluids. A .25" solid steel spacer was used at the top end except for saturated specimens, and then it was used on the bottom. Approximate dimensions of the cylinders were initially: 1.86" diameter, 4.0" length. All flat surfaces were ground using an 80 grit wheel. Wyoming Bentonite bought from Wards Scientific Supply was used (Na. Montmorillonite) and crushed Yule Marble was used as the calcite source. Both were reduced in grain size to extremely fine grain, almost ash-like. Quantities were weighed on the analytical balance and mixed for 20 seconds in the Bull Mill. One millimeter quantity was calculated using the formula for the area of a ellipse (conic section) and calculating the volume percent of minerals needed for each trial. Loss of gouge material during application was minimal.

The apparatus used is pictured in (Figure 4). It employs a variable speed mechanical loading system which compresses the rock specimen inside a constant volume pressure vessel. Confining pressure is applied to the oil in the vessel to achieve an external three-dimensional stress field ($\sigma_2 = \sigma_3$). Pore pressure is created by pressurizing the saturated specimen through the hollow upper piston.

All experiments were monitored by simultaneous force versus displacement graphs and, in addition, pore pressure versus displacement was monitored for saturated runs. Force/displacement graphs were later digitized and plotted as stress versus strain using the program listed in the appendix. No surface area corrections have been made on stress/strain data.

FIGURE 4. LSR AXIAL
LOADING APPARATUS AND
PRESSURE VESSEL INSERT



EXPERIMENTAL RESULTS

Mixtures of silt to clay in proportions of 0, 10, and 50% were observed in saturated dry loading tests using dilithologic specimens. The 100% calcite, dry, experiment was performed using Tennessee Sandstone only (Shimamoto).

Sharp transitions from elastic to inelastic deformation are present in the stress/strain curves for the dry 100% and both 50% clay runs. The 100% dry stress/strain shows an almost flat curve during sliding, while in the 100% saturated as well as in both 50% dry and saturated runs a linear work-hardening mode is indicated in later sliding behavior. Within this range also, the saturated runs exhibit an initial non-linear sliding mode and later linear, but work-hardening, sliding. No stress drop occurred in either 50% mixture experiment while stress drops were present in both 100% clay runs. Both the 100% and 50%, dry, clay experiments lack the initial non-linear portion; however, the similarity ends there. Later displacement in the 50% saturated mixture run produced a stress/strain curve parallel to that of the 50% dry experiment. A long-term, non-linear sliding mode also seems to be present in the 100% saturated run prior to achieving peak stress. A work-softening mechanism seems to be present in both 10% clay stress/strain curves prior to peak stress. Unfortunately, the dry 10% experiment is inconclusive of the gouge sliding behavior since the effective stress exceeded that of the maximum Berea strength. In this test, the Berea entered a transitional brittle-ductile strain; no sliding along the precut was evident in the specimen. Sliding did occur in the 10% saturated run, however, with the stress/strain curve being

essentially flat after a very small peak stress drop (@ several tenths of a MPa). Friction coefficients at the peak stresses varied greatly from .511 for 100% clay saturated to 1.3 for the 100% calcite, dry run. A list of coefficients for peak stresses is contained in (Table 1). Pore pressure changes during the sliding mode of saturated experiments were very small (increased). Displacement/time graphs did not provide enough resolution for detection of different displacement rates within each experiment. Attempts to impregnate dry specimens for thin-section were not successful in the time frame of this research.

RUN NO.	VOLUME % BENTONITE	PORE FLUID	MINERAL CONTENT	PEAK STRESS	FRICITION COEFF.
515	0%	dry		308.41 MPa	peak- 1.3000
843	10%	dry	bentonite- .439 g calcite- 3.960 g		
848	10%	wet	bentonite- .441 g calcite- 3.953 g	188.80 MPa	peak- 1.3401 sliding- 1.2310
558	50%	dry		81.70 MPa	peak- 1.0423
853	50%	wet	bentonite- 1.483 g calcite- 2.274 g	60.73 MPa	peak- .9517
840	100%	dry	bentonite- 2.964 g	56.68 MPa	peak- .9296 sliding- .9370
839	100%	wet	bentonite- 2.963 g	16.93 MPa	peak- .5109

NOTE: Increased value of frictional coefficient in sliding mode may be due to the decrease in apparent area of contact.

TABLE 1

Figure 5a. Stress and frictional coefficient versus axial shortening curve and stress accumulation rate curve are shown. The specimen was Berea and Tennessee Sandstones with 1 mm of pure, dry, bentonite gouge along a 35° precut.

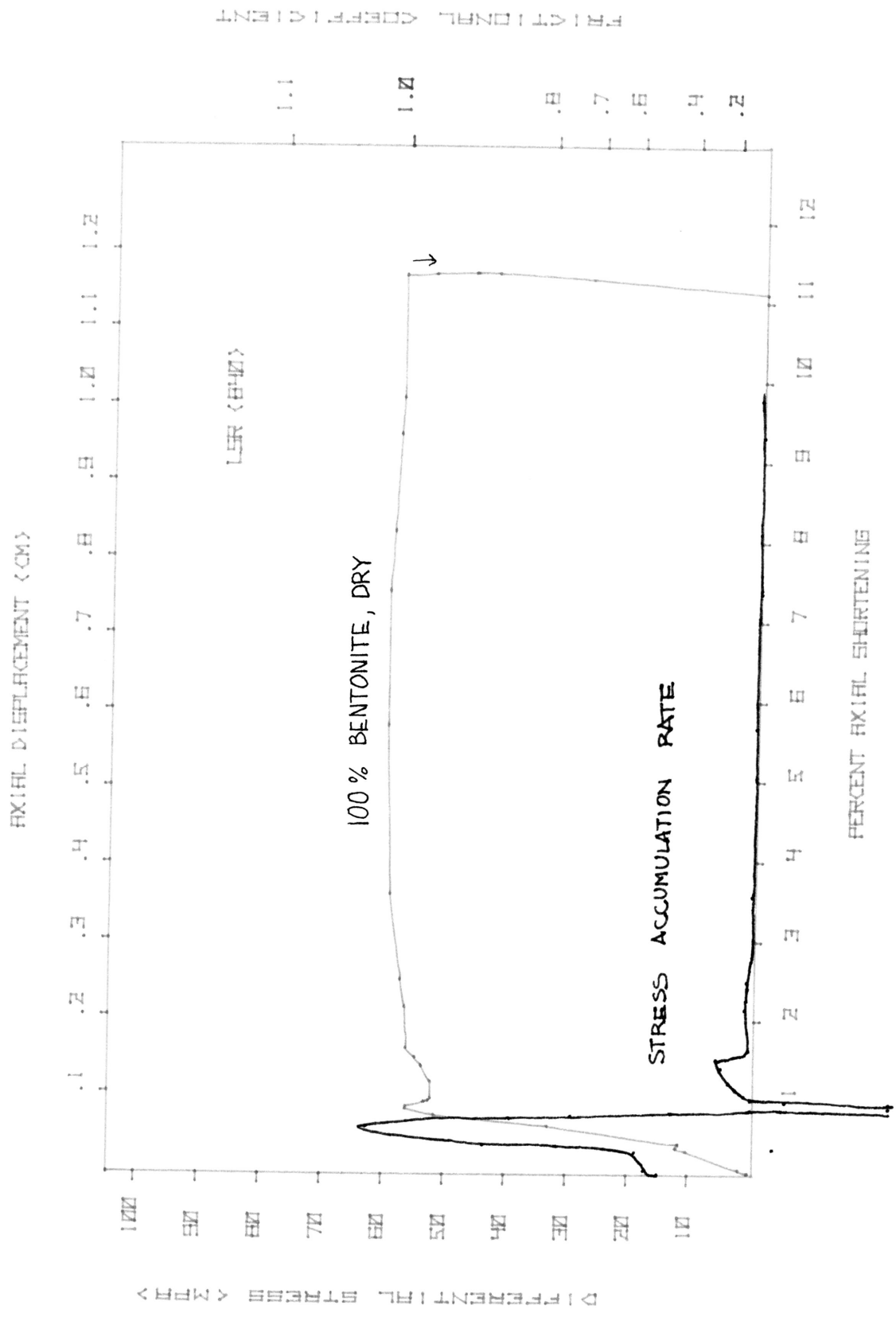


FIGURE 5a

Figure 5b. Stress and frictional coefficient versus axial shortening curve and stress accumulation rate curve are shown. The specimen was Berea and Tennessee Sandstones with 1 mm of pure, saturated, bentonite gouge along a 35° precut.

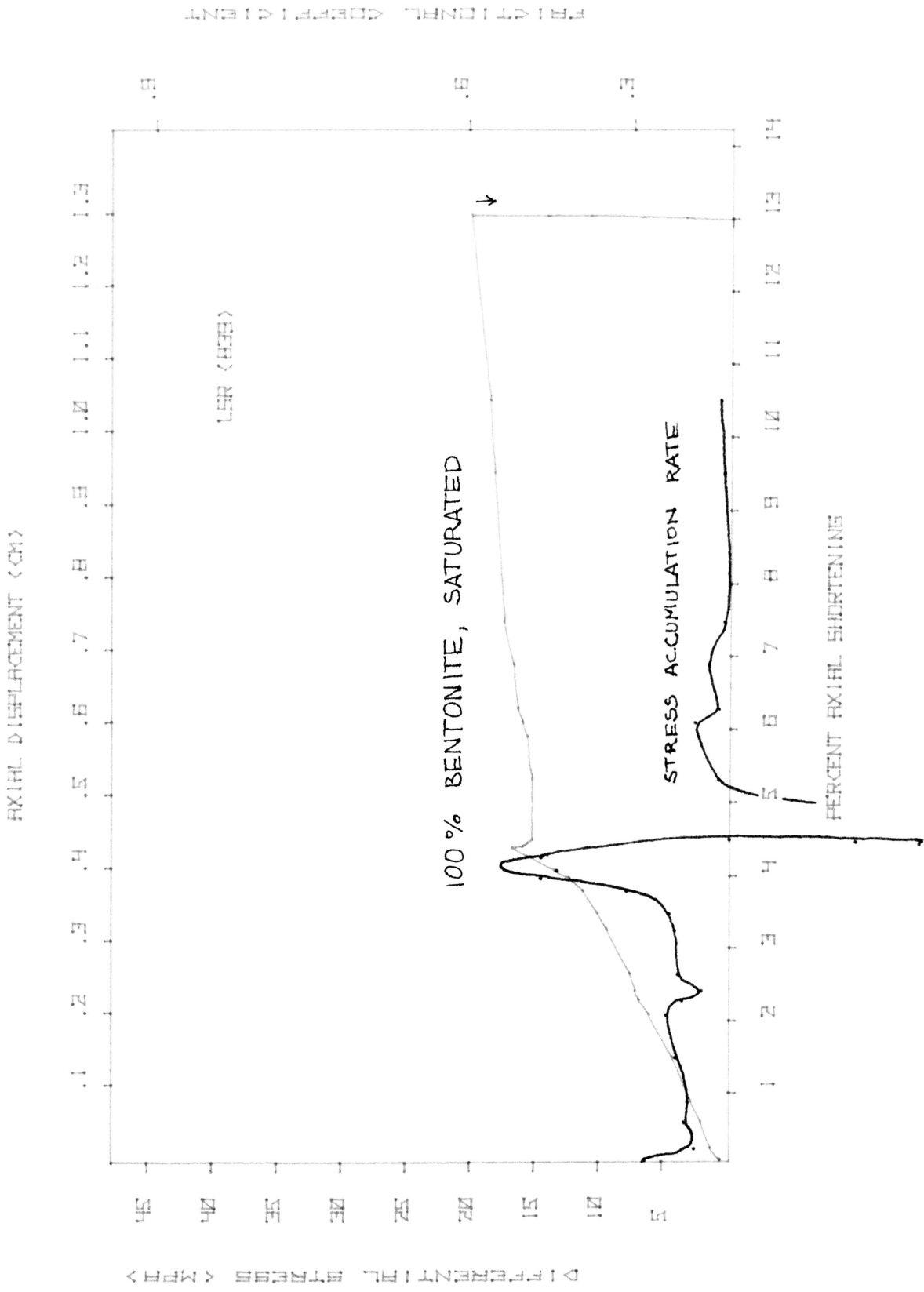
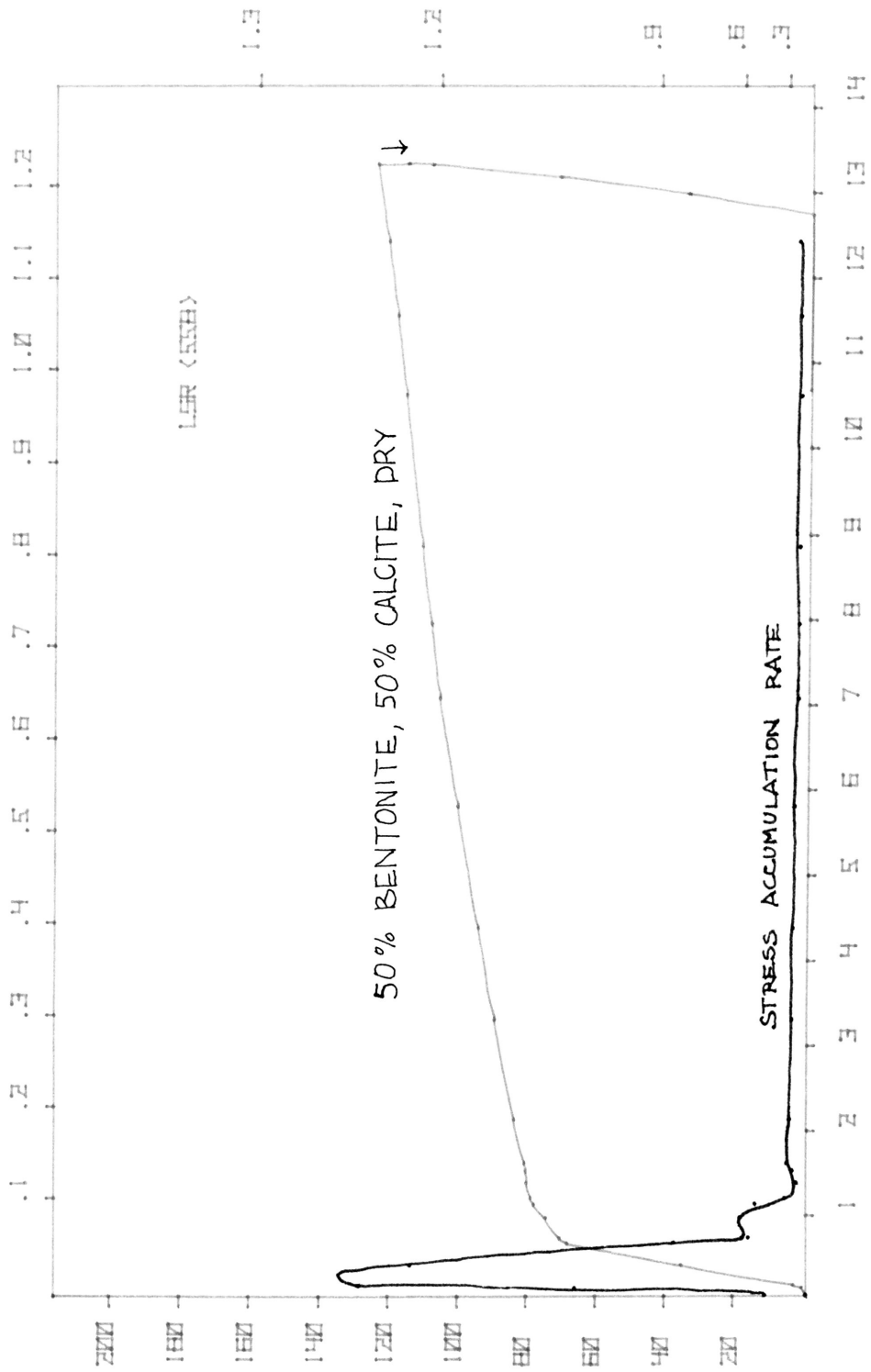


FIGURE 5b

Figure 6a. Stress and frictional coefficient versus axial shortening curve and stress accumulation rate curve are shown. The specimen was Tennessee Sandstone with 1 mm of dry, 50% bentonite, 50% calcite gouge along a 35° precut.

AXIAL DISPLACEMENT (CM)



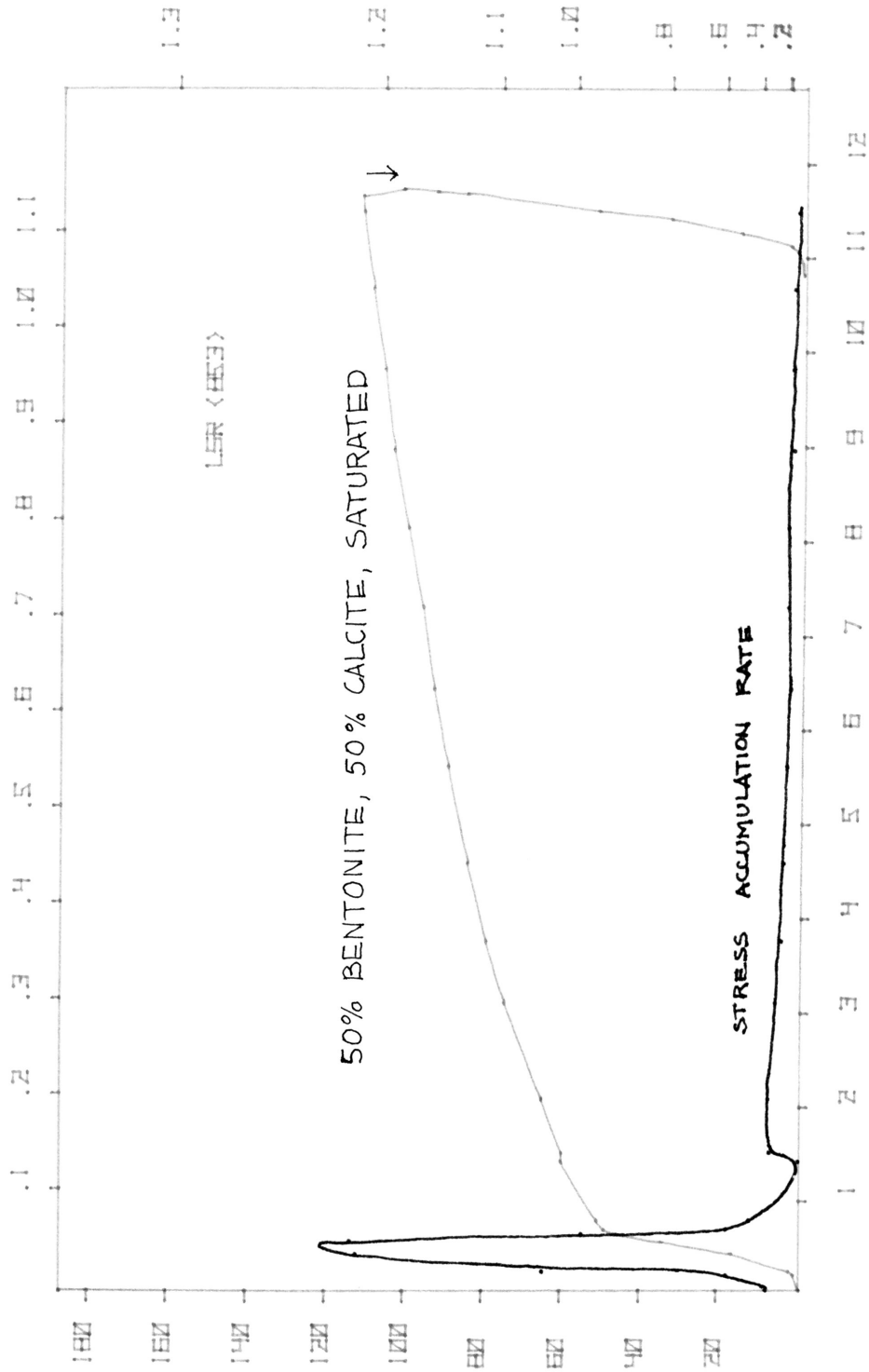
AXIAL DISPLACEMENT (CM)

PERCENT AXIAL SHORTENING

FIGURE 6a

Figure 6b. Stress and frictional coefficient versus axial shortening curve and stress accumulation rate curve are shown. The specimen was Berea and Tennessee Sandstones with 1 mm of saturated, 50% bentonite, 50% calcite gouge along a 35° precut.

AXIAL DISPLACEMENT (CM)



PERCENT AXIAL SHORTENING

FIGURE 6b

Figure 7a. Stress versus axial shortening curve and stress accumulation rate curve are shown. The specimen was Berea and Tennessee Sandstones with 1 mm of dry, 10% bentonite, 90% calcite gouge along a 35° precut.

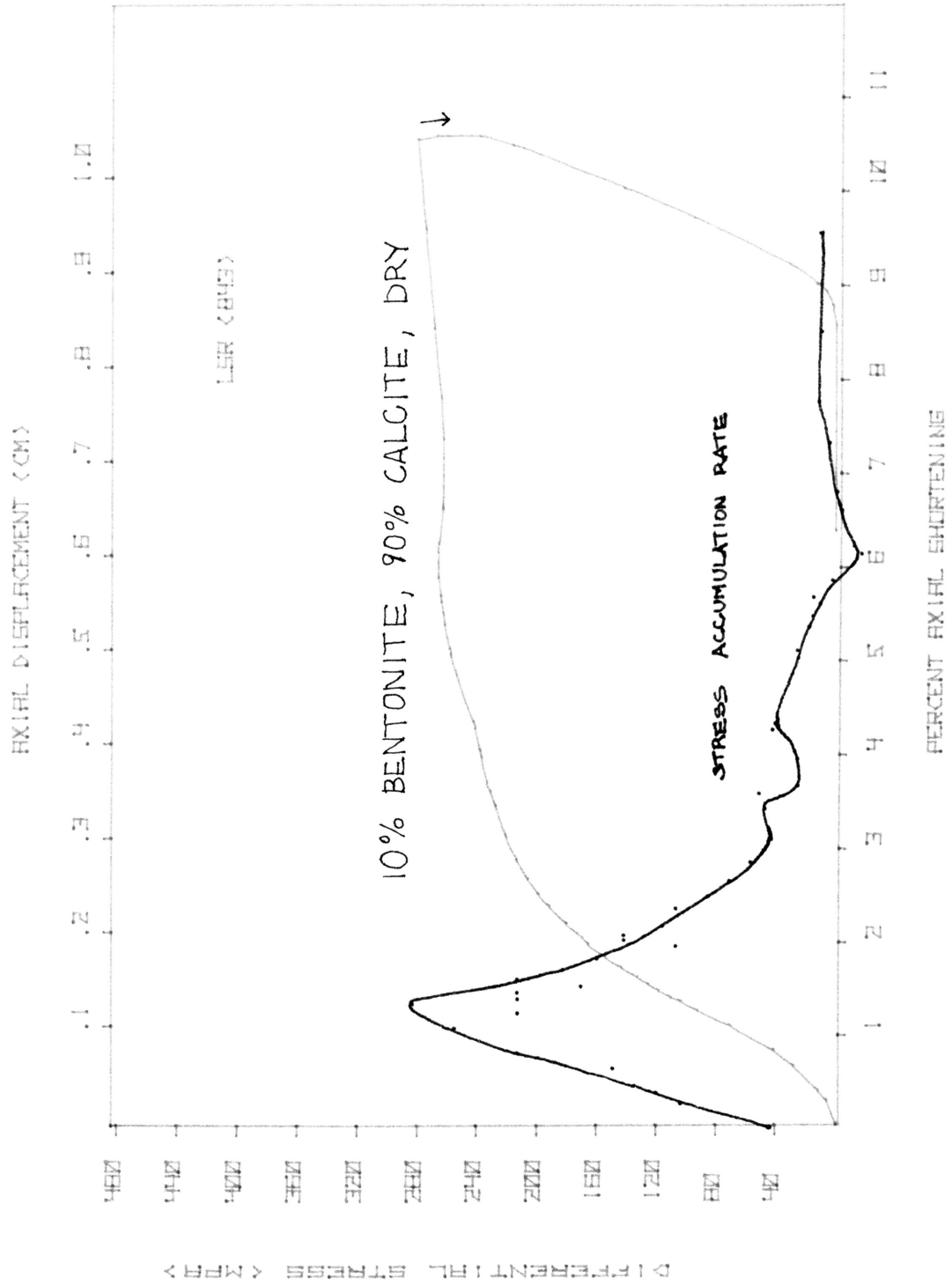


FIGURE 7a

Figure 7b. Stress and frictional coefficient versus axial shortening curve and stress accumulation rate curve are shown. The specimen was Berea and Tennessee Sandstone with 1 mm of saturated, 10% bentonite, 90% calcite gouge along a 35° precut.

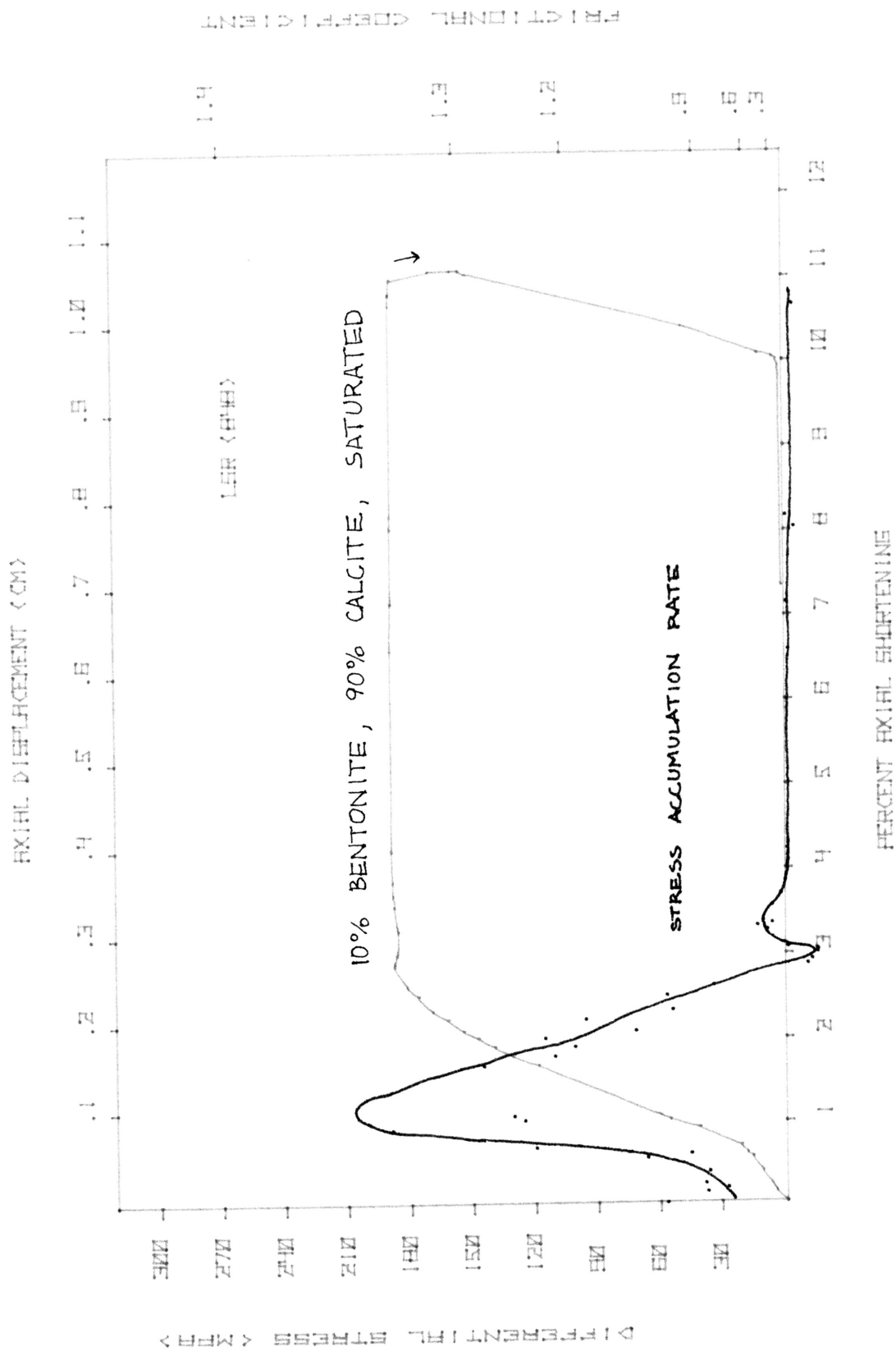


FIGURE 7b

Figure 8. Stress and frictional coefficient versus axial shortening curve for Tennessee Sandstone specimen with a 1 mm thick layer of pure, dry, calcite gouge along a 35° precut (Shimamoto, 1976).

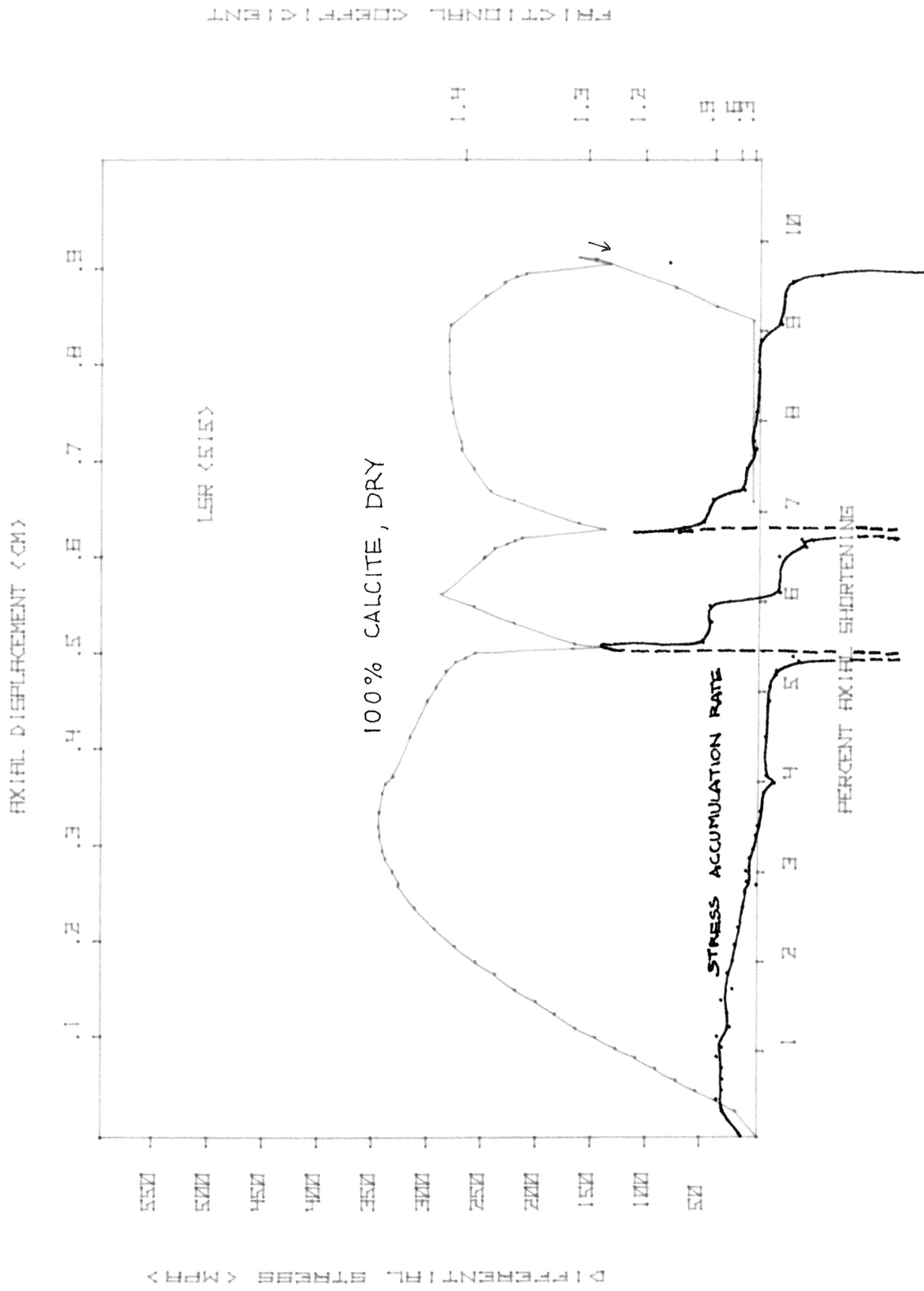
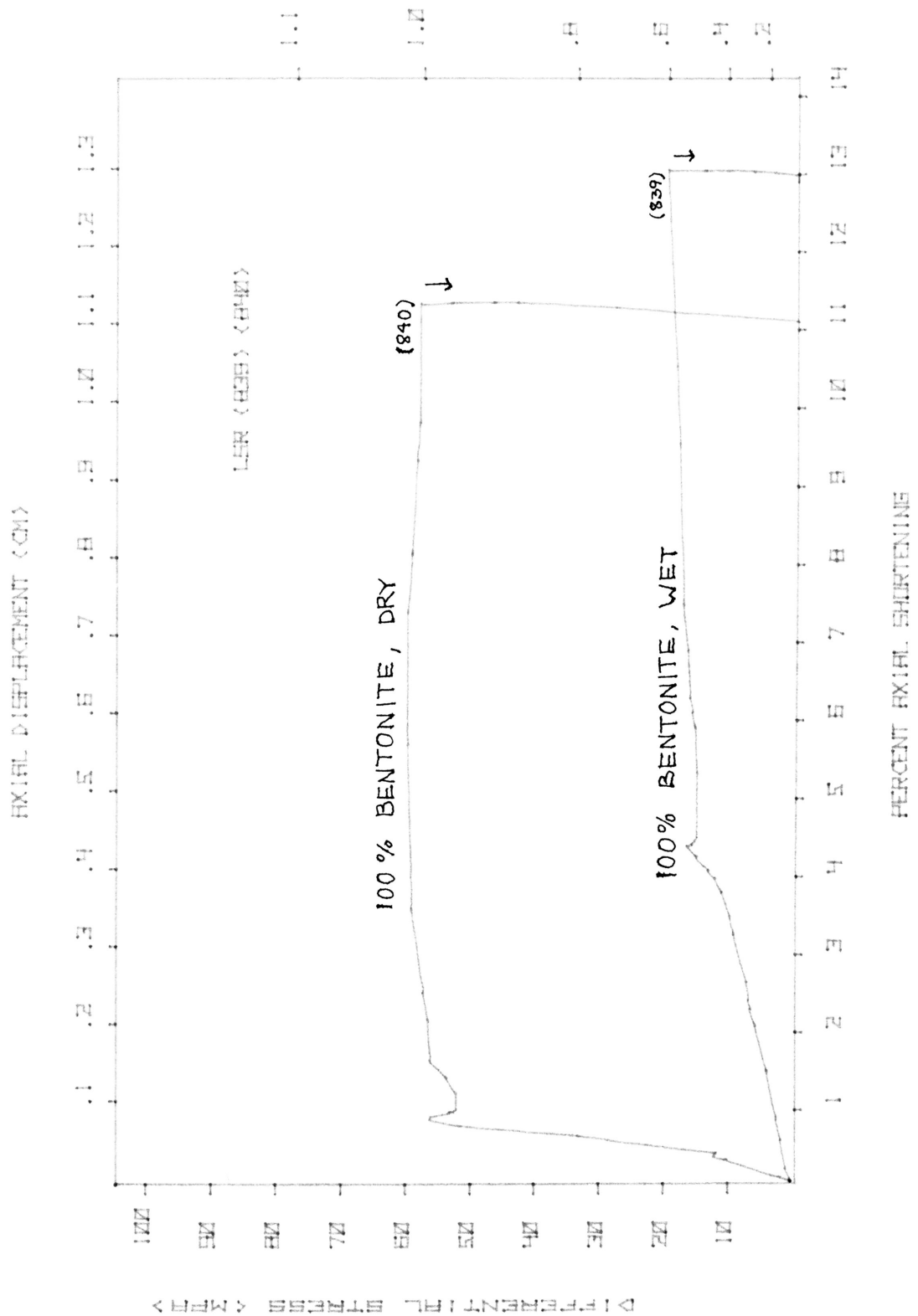


FIGURE 8

Figure 9. Stress and frictional coefficient versus axial shortening curves for 1 mm, 100% bentonite gouge saturated (LSR 839) and dry (LSR 840). The specimens were Berea and Tennessee Sandstones with a 35° precut.

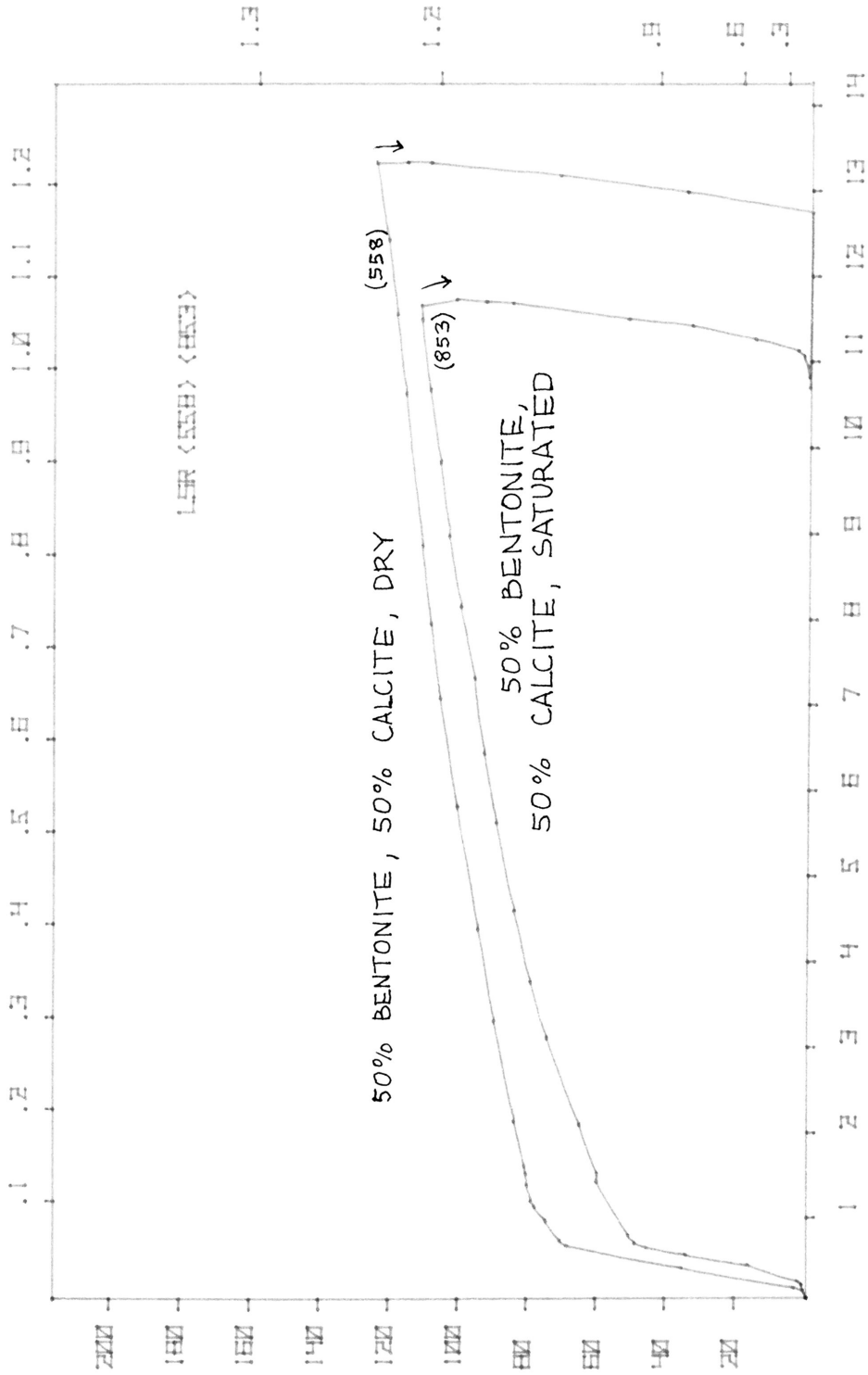


AXIAL DISPLACEMENT (CM)

FIGURE 9

Figure 10. Stress and frictional coefficient versus axial shortening curves for 1 mm, 50% bentonite, 50% calcite gouge saturated (LSR 853) and dry (LSR 558). The specimens were Berea and Tennessee Sandstones with a 35° precut.

AXIAL DISPLACEMENT (CM)



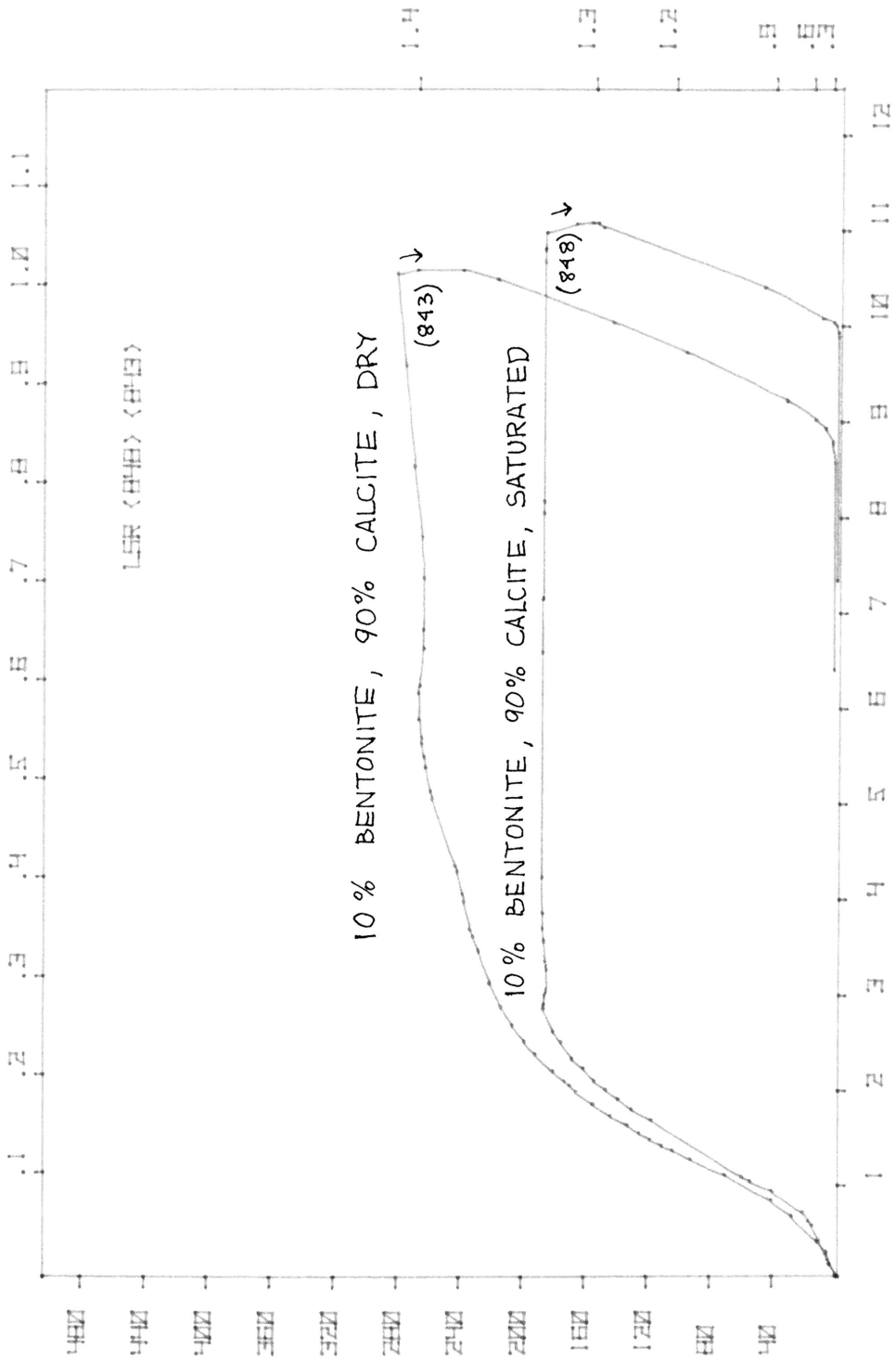
AXIAL DISPLACEMENT (CM)

PERCENT AXIAL SHORTENING

FIGURE 10

Figure 11. Stress versus axial shortening curves for 1 mm, 10% bentonite, 90% calcite gouge saturated (LSR 848) and dry (LSR 843). Frictional coefficient values apply only to the saturated run. The specimens were Berea and Tennessee Sandstones with a 35° precut.

AXIAL DISPLACEMENT (CM)



UNITED STATES GEOLOGICAL SURVEY

15R (848) (843)

10% BENTONITE, 90% CALCITE, DRY
10% BENTONITE, 90% CALCITE, SATURATED

PERCENT AXIAL SHORTENING

UNITED STATES GEOLOGICAL SURVEY

FIGURE 11

Figure 12. Stress and frictional coefficient versus axial shortening curves for 1 mm, dry gouges of varying compositions.

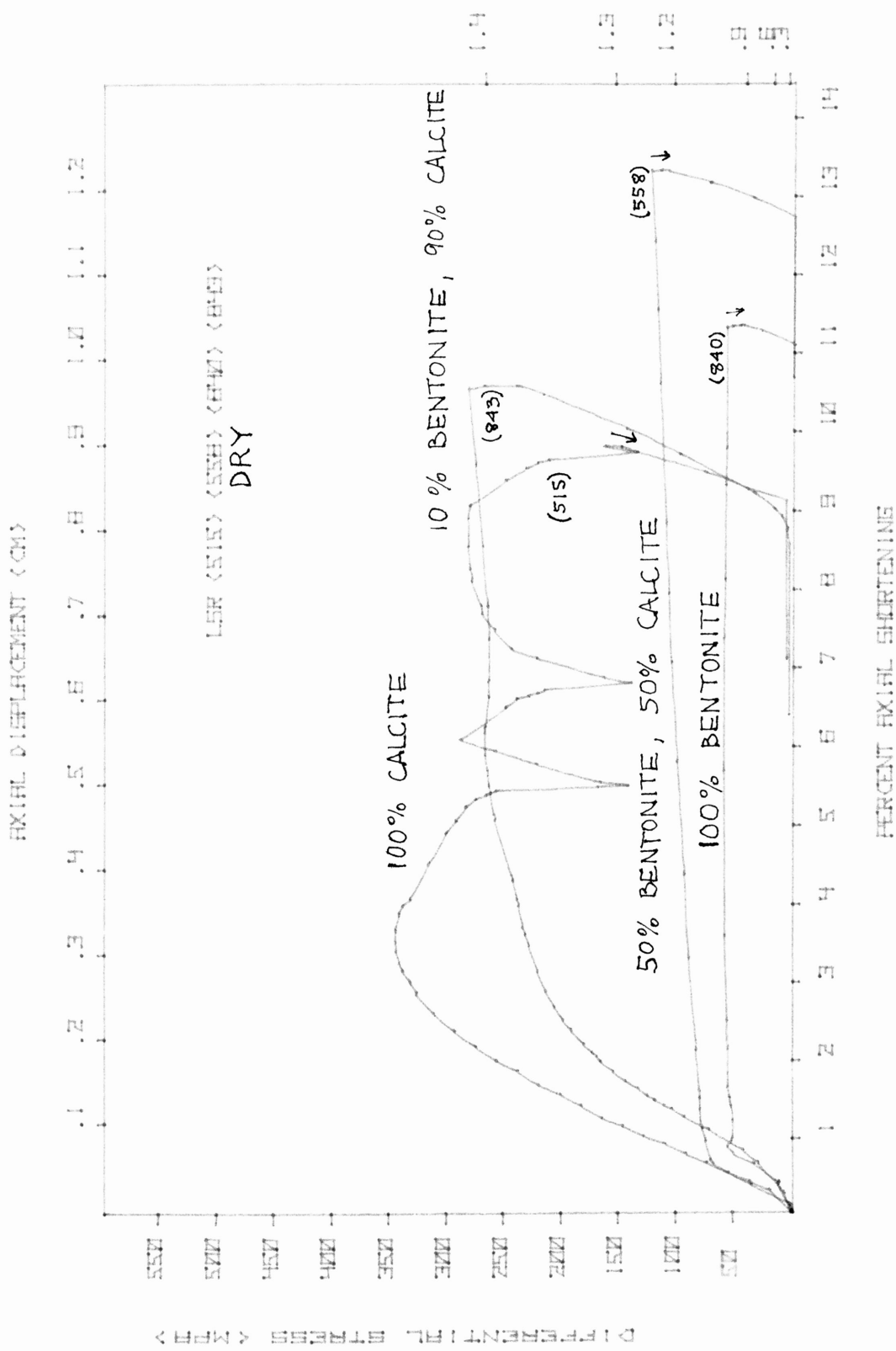
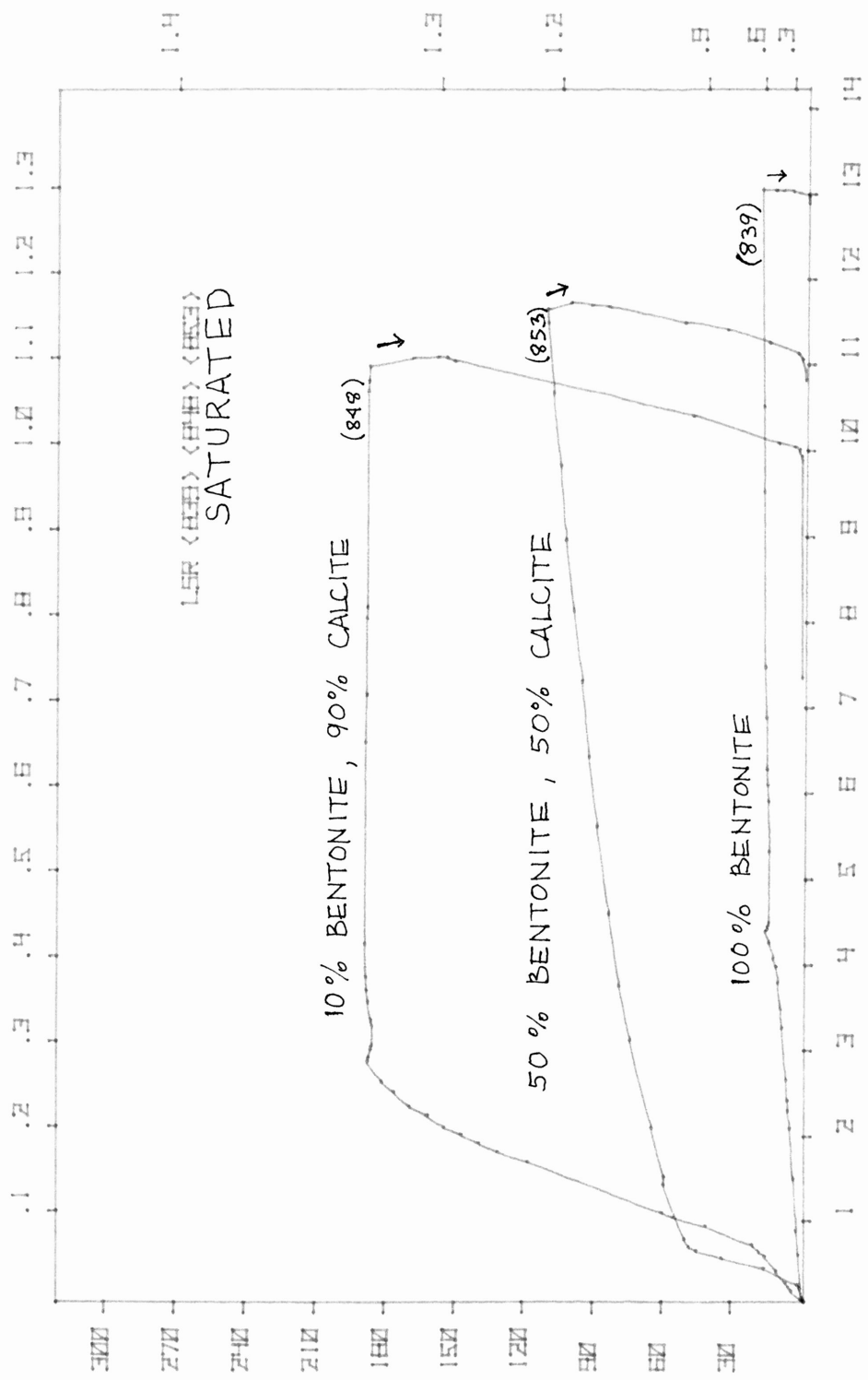


FIGURE 12

Figure 13. Stress and frictional coefficient versus axial shortening curves for 1 mm, saturated gouges of varying compositions.

AXIAL DISPLACEMENT (CM)



SATURATED

10% BENTONITE, 90% CALCITE

50% BENTONITE, 50% CALCITE

100% BENTONITE

PERCENT AXIAL SHORTENING

FIGURE 13

DISCUSSION OF RESULTS

This research has brought to light several factors of deformation, in gouges containing Montmorillonite, which influence the behavior of precut specimens. Although these factors appear to have definite relationships to one another, no attempt has been made here to quantify or isolate them.

The presence of at least 10% bentonite in the homogeneous, saturated silt-clay gouge is enough to impose stable sliding behavior on precut specimens under moderate confining pressure. The initial yield strength of the calcite dominated the pre-sliding frictional characteristics, however, upon initiation of sliding, bentonite caused the friction to remain stable, yet quite high. All experiments containing a silt-clay gouge exhibited a pre-sliding elastic and/or work-softening behavior characteristic of calcite. During sliding, the displacement was very stable for all mixtures except for slight nonlinearities in the stress/strain curves of saturated specimens. It is supposed that these nonlinearities may be explained by the release of weakly held interlayer water which is released through shear displacement. More evidence of the effect of interlayer water on pure, saturated clay are the regions of the stress/strain curve prior to and after the peak stress for 100% bentonite. Bombolakis (1978) suggests that the nonlinear behavior of clays may be due to electro-viscous sliding during the initial phases of deformation. We would expect a slowly building frictional resistance, as water is released, culminating in a stress drop. This is the behavior observed, although Bombolakis has in no way quantified his descriptions and therefore no conclusions can be made here on that

basis.

A work-hardening sliding behavior was shown in both 50% bentonite runs. This may indicate a relatively homogeneous deformation within the gouge involving frictional contact between grains of calcite and bentonite. Possible grain size reduction of the clay platelets within the gouge is responsible for the work-hardening. Very flat stress/strain curves characterize the sliding of 100% dry and 10% wet bentonite experiments. Perhaps this behavior is due primarily to slip at the gouge-rock interface instead of involving internal deformation of the gouge. In the 10% bentonite, saturated run, this type of deformation seems plausible due to the lack of a significant percentage of weak minerals and water within the gouge. The dry, 100% bentonite run may not be characteristic of high percentages of clay, however. Two factors may have a hand in bearing out this opinion. First, in saturated experiments the confining pressure was applied fully prior to application of pore pressure. This may have allowed the gouge layer to become essentially impermeable to any external introduction of water. Therefore, the confining pressure on the gouge would have been the effective confining pressure on the specimen plus the pore pressure within the specimen. We might expect a greater frictional contact between grains and consequently a higher coefficient of friction within the gouge than might be expected. The second factor which might explain the stability of the 100% dry experiment is simply that there weren't sufficient silt grains within the gouge to grind the platelets down, which increases the friction with increasing displacement. Indeed, clay content in the 50% bentonite experiments seems to enhance the homogeneous

deformation of the gouge, so that it is unlikely that displacement in the 100% run was only along the interface.

Sliding behavior in the 50% tests is perhaps the most diagnostic of the effects of saturated versus unsaturated clays. It may indicate that enough water was eliminated from the saturated layer to produce a gouge whose plasticity was essentially the same as the dry gouge. Note that both runs are essentially the same except for magnitude and a non-linear transition zone in the saturated run. The lack of a stress drop in these runs may be caused by the much greater frictional strength of the calcite absorbing the greater load upon failure of the clay fraction. The same could be inferred for the very small drop in the saturated 10% bentonite run.

Many limitations may be placed upon the conclusions offered here, none of which are less important than the lack of tests for reproducibility. However, several other uncertainties remain in the description of mechanics preceding. In saturated specimens containing a high percentage of clay, the permeability may be considered extremely low, if not non-existent over the time frame of these experiments. Combined with the layered effect of grain size reduction at the gouge-rock boundary and compaction, the possibility of having local failure of pressure cells of trapped water is greatly enhanced. Since this is an inhomogeneous effect and the Bombolakis model is based on homogeneous deformation within the gouge, the implications of this mechanism is not yet clear. Another effect that may have influence the behavior of saturated clay was saturating the gouge prior to confining it. This would enhance the mobility of the clay sheets to achieve the 'cardhouse' structure of

electrical equilibrium prior to loading. The same high water content may negate this effect upon compaction by escaping the gouge zone and rotating the sheets in a laminar flow.

By using Berea Sandstone as the upper member in the specimens, unknown factors of deformation are introduced along the interface with the build-up of high differential stresses. This effect may be better resolved in research with rock-on-rock dilithologic specimens.

Summary - Conclusion

The following points are suggested as explanations or weaknesses of this research.

- 1.) Unsaturated silt-clay gouges offer stable frictional resistance to the extent that the sheet structures are able to interact with one another, not blocked laterally by silt particles, thus preventing a 'locked' frictional contact to dominate the resistance to shear stress.
- 2.) Saturated silt-clay gouges produce even greater stability and weaker frictional resistance but behave very similarly to unsaturated gouges after an initial non-linear sliding mode. Peak shear stress reduction in the saturated state seems much greater than the reduction of the sliding frictional stress.
- 3.) Relatively homogeneous deformation seems to occur in saturated and unsaturated silt-clay mixtures for 50% clay content and more. Grain size reduction of clay particles within the gouge accounts for the substantial work-hardening of the sliding mode in both saturated and unsaturated tests.
- 4.) Factors which should be further isolated include:
 - a. The interaction between the frictional characteristics of clay and silt at the interface and inside the gouge zone.
 - b. Effect of the peak yield stress of the silt fraction on the homogeneity of gouge deformation.
 - c. Inhomogeneous structural failure associated with pressure-cell failure or other mechanisms.
 - d. Isolation of a sliding mode prior to peak stress in very

high clay concentration saturated gouges.

e. Effect of the weaker rock (Berea) on the initial yield characteristics of high silt content gouges.

Microscope study is essential in isolating the deformation mechanisms involved in these tests. Increased resolution of the non-linearities in some saturated stress/strain curves should be helpful in describing the transition from electro-viscous to frictional shear.

Appendix

STRESS/STRAIN PROGRAM
(Hewlett-Packard 9820A)

```

0: ENT "STRAIN%/IN",R1001,"MAX STRAIN (IN)",X,"FORCE/IN (LB)",B
1: ENT "MAX FORCE (IN)",Y,"L(O) (IN)",R990,"RADIUS",C→R995,"P(C)",
  R988
2: B/145.5→R1002;2YR1002/C↑2π→Y;R1001X→X;0→R1004→R1005→R989
3: ENT "STRAIN-TIC",A→R993,"STRESS-TIC",B→R997;X+A→X
4: SCL -2A,X+2A,-Y/4,Y;INT (Y-2B)→R992;FXD 0;X→R996;FLT
5: ENT "MIN REG NO.",R1000→C
6: PLT 0,R992;PLT 0,0;PLT R996,0;PLT R996,R992;PLT 0,R992;PEN ;
  B→C
7: LTR 0,C,112;FXD 0;PLT 1;FLT ;LTR -.8A,C,211;FXD 0;PLT C;FLT ;
  B+C→C;IF R992>C;JMP 0
8: A→C;LTR -1.5A,Y/5,122;PLT "DIFFERENTIAL STRESS (MPA)"
9: LTR C,0,113;FXD 0;PLT 1;FLT ;LTR C,-.7B,211;FXD 0;IF A≠INT A;
  FXD 1
10: PLT C;FLT ;A+C→C;IF R996>C;GTO -1
11: LTR R996/3,-1.7B,211;PLT "PERCENT AXIAL SHORTENING"
12: LTR R996/3,R992+1.4R997,211;PLT "AXIAL DISPLACEMENT (CM)"
13: 2.54R990R996/100→B;R996/B→B;.1B→C
14: LTR C,R992,111;FXD 0;PLT 1;FLT ;LTR C,R992+.4R997,211;FXD 1;
  FLT C/B;FLT
15: .1B+C→C;IF R996-.1B>C;GTO -1
16: ENT "SLIDING?",Z;IF Z;ENT "SAWCUT ANGLE",R989
17: IF Z=0;JMP 5
18: LTR R996+1.65R993,Y/5,122;PLT "FRICTIONAL COEFFICIENT";.3→C
19: IF R992≤200;.2→C;SFG 4;IF R992≤100;.1→C;SFG 5

```

```

20: 2CR988/(1-CTAN R989)SIN (2R989)→A
21: IF A>R992;JMP 5
22: LTR R996,A,114;FXD 0;PLT 1;FLT ;LTR R996+.4R993,A,211;FXD 1;
    PLT C;FLT
23: IF FLG 4(1>C);GTO -3;.2+C→C;IF FLG 5;C-.1→C
24: IF 1>C;.3+C→C;IF C≤1.5;GTO -4
25: .1+C→C;IF C≤1.5;GTO -5
26: ENT "NO. OF RUNS",Z;Z+1→Z;LTR X-INT (2+ZR993),Y-4R997,211;
    PLT "LSR "
27: ENT "RUN NO.?",Z;IF Z;FXD 0;PLT "(";PLT Z;PLT ")";PRT "LSR",Z
    FLT ;JMP 0
28: "D";R1000→C;ENT "PLOT PEN",Z,"ENTER DATA?",Z;IF Z;JMP 3
29: ENT "LOAD DATA?",Z;IF Z;ENT "FILE NO.",Z;LDF Z
30: GTO "PLOT"
31: PRT "ENTER","STRAIN,FORCE","(1ST X,1ST Y)","TO INDICATE",
    "END OF DATA"
32: SPC 8;ENT "1ST X",R998→RC,"1ST Y",R999→R(C+1);C+2→C
33: "SS";ENT "STRAIN",RC,"F",R(C+1);RC-R998→RC;R(C+1)-R999→R(C+1)
34: R1001RC→RC;R1002R(C+1)/R995↑2π-R(C+1)
35: IF RC≠0;C+2→C;GTO "SS"
36: FXD 0;PRT "MAX REG NO.",C;FLT;SPC 2
37: "PLOT";R1000→C;CFG 1;ENT "LINE=0,DOT=1",Z;IF Z;SFG 1
38: "F";IF R989R(C+1);1/(2R988/R(C+1)SIN (2R989)+TAN R989)→R991
39: IF FLG 3;GTO "C"
40: IF R991>R1005;R991→R1005
41: PLT RC,R(C+1);IF R(C+2)≠0;C+2→C;IF FLG 1;PEN
42: IF R(C+2)=0;PLT RC,R(C+1);JMP 2

```

```
43: GTO "F"; IF (R1005>R991)RCR(C+3)(0≤C-6); C-6→C; R991→R1003; SFG 3
44: PEN ; ENT "DERIVATIVE PLOT?", Z
45: GTO "M"; IF Z; ENT "PEN", Z; SFG 14; 0→R1009; R1000→C; GTO "DP"
46: "DP"; (R(C+3)-R(C+1))/(R(C+2)-RC)→R1010
47: IF (ABS R1010>R1009)(R1010≠1/0); ABS R1010→R1009
48: GTO "DP"; IF R(C+4)≠0; C+2→C; IF RC>X-2; JMP 1
49: R1000→C; Y/2R1009→Y
50: IF R(C+2)>RC; PLT RC, (R(C+3)-R(C+1))Y/(R(C+2)-RC); PEN
51: IF R(C+4)≠0; C+2→C; GTO -1
52: "M"; PRT "-----"
53: ENT "MORE PLOTS?", Z; GTO "END"; IF Z; ENT "MIN REG NO.", R1000;
GTO "D"
54: "C"; IF R989(R991≤R1005); FXD 4; PRT "STRAIN%", R(C+2), "COEF
FICIENT", R1005; FLT ; SPC
55: C+6→C; CFG 3; GTO "F"; R1003→R1005
56: "END"; IF R989; SPC 7
57: DSP "END"; END
```